JOURNAL OF GEOPHYSICAL RESEARCH, VOL. 92, NO. B12, PAGES 12,629-12,648, NOVEMBER 10, 1987

SOURCE PARAMETERS FOR 11 EARTHQUAKES IN THE TIEN SHAN, CENTRAL ASIA, DETERMINED BY P AND SH WAVEFORM INVERSION

Michael R. Nelson, Robert McCaffrey, and Peter Molnar

Department of Earth, Atmospheric, and Planetary Sciences, Massachusetts Institute of Technology, Cambridge

Abstract. The Tien Shan mountain belt of central Asia was formed in late Paleozoic time and reactivated in Tertiary time following the collision of India with Eurasia, more than 1500 km to the south. To study the style and distribution of faulting occurring today in the Tien Shan, we digitized long-period World-Wide Standard Seismograph Network P and SH waveforms of 11 of the largest Tien Shan earthquakes between 1965 and 1982 and then used a least squares inversion routine to constrain their fault plane solutions and depths. Four of the earthquakes occurred near the southern edge of the Tien Shan, and two occurred in the intermontane Fergana Basin. These earthquakes occurred at depths of 10-20 km and are associated with thrust faulting on east-west to southwest-northeast striking fault planes that dip moderately (35°-55°). The other five earthquakes, in the northern Tien Shan, were mostly deeper (15-44 km), and the fault plane solutions of four of them are similar to the events farther south. The exception, an event on June 2, 1973, probably occurred on a gently northward dipping, east-west striking fault plane. All events occur within the basement at depths of 10 km or greater. Waveforms for earthquakes near the edges of the Dzungarian, Fergana, and Kucha basins are fit best using velocity structures with thick sediment layers, implying that sediments from these basins have been and are being underthrust beneath the neighboring mountains. We examined only the relatively small (m_b = 5.5-6.2) events after 1965 and did not study any of the largest events (M_s > 8) that occurred in the Tien Shan earlier in this century. Still, we can conclude that north-south shortening is presently occurring in the Tien Shan, with the formation of basement uplifts flanked by moderately dipping thrust faults. The present-day tectonics of the Tien Shan seem to be analogous to those of the Rocky Mountains in Colorado, Wyoming, and Utah during the Laramide orogeny in Late Cretaceous and Early Tertiary time.

Introduction

The Tien Shan in northwestern China and Soviet central Asia is one of the world's most rapidly deforming intracontinental regions. The mountain belt stretches east-west more than 2000 km, and in places elevations exceed 7000 m with many ranges higher than 5000 m (Figure 1). The present belt overlaps part of a Paleozoic orogenic belt that was reactivated in Tertiary time following the collision of India with Eurasia more than 1500 km to the south. The region is seismically quite active, producing several earthquakes with M_s > 8 since 1900. Since 1965 there have been more than a dozen earthquakes with body wave magnitudes ≈ 6. Here we examine these later events in order to understand better how intracontinental deformation is occurring in the Tien Shan.

Paper number 7B6019.
0148-0227/87/007B-6019$05.00

Crustal deformation in the interior of continents is generally more complex and diffuse than that occurring at plate margins. At mid-ocean ridges and in subduction zones, seismicity and active deformation are confined to rather narrow zones. In contrast, intracontinental deformation like that in the Tien Shan, in the Atlas Mountains of north Africa, in the Basin and Range Province, or in Turkey is diffuse, and the related seismicity is much more complex. Typically, the level of seismicity and the style of deformation vary markedly over distances of tens of kilometers.

Most continental regions with significant seismic activity are near active or recently active plate boundaries (e.g., the Himalaya, California, or the East African Rift Zone). In contrast, seismicity in the Tien Shan occurs more than 1500 km north of the nearest recent plate boundary, the Indus-Tsangpo Suture Zone just north of the Himalaya. The Tertiary shortening in the Tien Shan has been entirely within what was the Eurasian plate before its collision with India; there are no known Tertiary ophiolites or pelagic sediments to indicate the subduction of oceanic crust near the Tien Shan in Tertiary time. The Tien Shan can be compared to other regions where intracontinental shortening has occurred in the past, like the Rocky Mountains.

Tectonic Setting

The Tien Shan consists mainly of Paleozoic sedimentary rocks folded and faulted during the Carboniferous and Permian periods [Burtman, 1975] when slip on gently dipping, east-west striking thrust faults accommodated north-south shortening. In addition, a number of northwest-southeast trending right-lateral faults (e.g., the Talasso-Fergana fault) apparently were active. Since the collision of India and Eurasia in Tertiary time many of these strike-slip faults have been reactivated [Burtman, 1980; Leith, 1986; Suvorov, 1963; Trifonov, 1978; Wallace, 1976], and north-south shortening is again being accommodated along east-west trending thrust faults, producing the east-west trending block uplifts seen today. Geologic mapping and Landsat imagery indicate that many of these uplifts are flanked on both their north and south sides by thrust faults that dip beneath the mountains [Tapponnier and Molnar, 1979].

The actively deforming Tien Shan is flanked by the relatively aseismic Siberian Shield and Dzungarian Basin on the north and the stable Tarim Basin on the south (Figure 1). The low

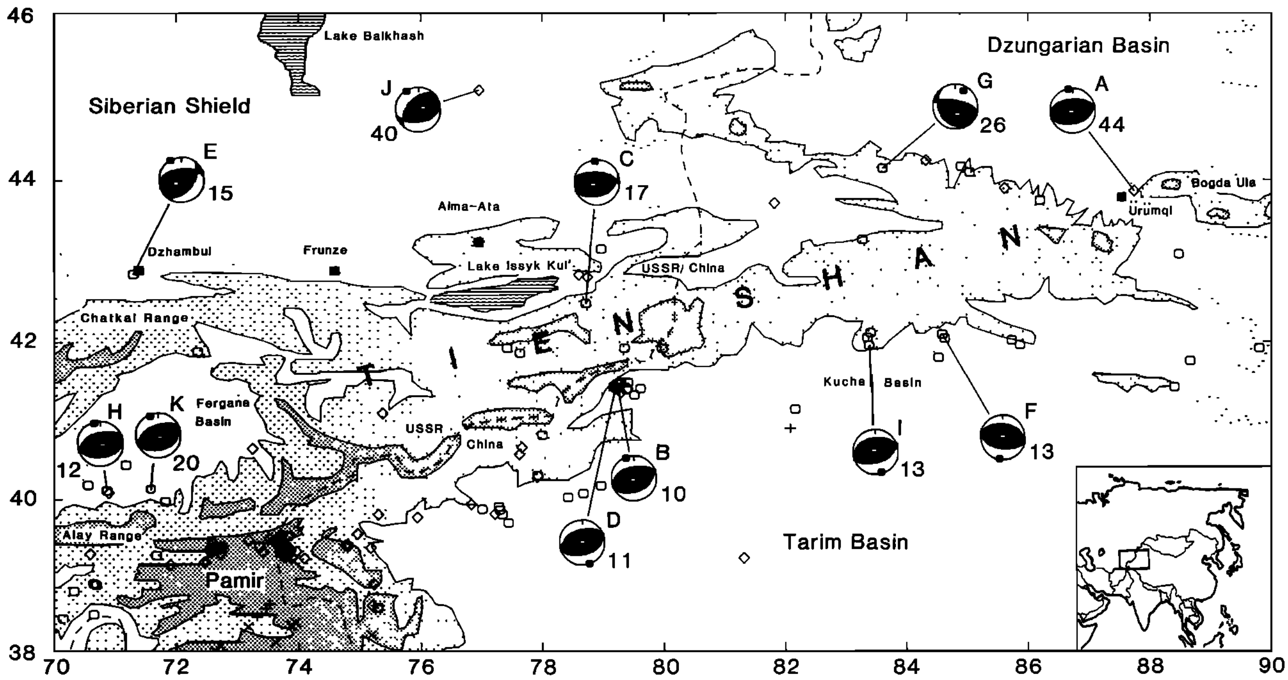

Fig. 1. Summary map of the Tien Shan showing the ISC epicenters and fault plane solutions of the 11 earthquakes studied. The fault plane solutions show thrust and oblique thrust faulting occurring primarily on east-west trending range-bounding faults. The dashed line marks the USSR-China border. The 1000-m contour is dotted. Regions with elevations >2000 m are stippled, and regions above 4000 m are shaded. For each fault plane solution (Table 1) the lower hemisphere equal-area projection of the focal sphere is shown with the compressional quadrants shaded. Next to each focal mechanism are an identifying letter and the centroid depth in kilometers. Also shown are ISC epicenters for earthquakes occurring between 1971 and 1981 with $m_b > 5.0$. Symbols plotted indicate focal depths, h, reported by the ISC: square, $h < 33$ km; diamond, $33 \text{ km} < h < 70$ km; plus, $70 \text{ km} < h < 100$ km; cross, $h > 100$ km.

levels of seismicity, little relief, and low elevations (<1000 m) in the Tarim Basin were attributed by Molnar and Tapponnier [1981] to the presence beneath the Tarim Basin of cold, strong Precambrian shield that has been relatively unaffected by the deformation occurring both in the Tien Shan to the north and the Tibetan Plateau to the south.

Little geologic mapping or geophysical work from the Tien Shan has been published. In the early part of this century a number of expeditions in the Tien Shan made geologic traverses across parts of the region, collecting stratigraphic and paleontological data [Dmitriyev et al., 1935; Gröber, 1914; Norin, 1937, 1941]. Because of the inaccessibility of the region, much of the more recent work done on the Tien Shan has relied upon Landsat imagery and seismograms recorded at stations of the World-Wide Standard Seismograph Network (WWSSN) [Molnar et al., 1973; Ni, 1978; Tapponnier and Molnar, 1979; Vilkas, 1982]. First-motion fault plane solutions using WWSSN seismograms indicate that thrust faulting predominates in the Tien Shan but the strikes of the nodal planes are poorly constrained. Vilkas [1982] analyzed long-period teleseismic P waveforms for six earthquakes in the Tien Shan and found that all six events are characterized by thrust or oblique thrust faulting. Unfortunately, the P waveforms alone do not tightly constrain the strike of the nodal planes. Vilkas also confirmed that in the Tien Shan, faulting occurs down to depths of 45 km or greater [Chen and Molnar, 1977]. In the western Tien Shan, Soviet workers have operated about 20 regionally distributed seismic stations that provide data that have been used to locate earthquakes, to determine their first-motion fault plane solutions, and to make preliminary seismic velocity models for the region [Vinnik and Saipbekova, 1984; Wesson et al., 1975]. Unfortunately, most of the data from these stations are unavailable to us.

Technique

In order to learn more about the tectonics of the Tien Shan we matched synthetic seismograms to WWSSN long-period P and SH waveforms to constrain both the depths and the fault plane solutions of all 11 earthquakes in the Tien Shan that were well-recorded by the WWSSN between 1965 and 1983. Three other earthquakes with $m_b \approx 6$ (0952, March 23, 1971; July 26, 1971; and March 24, 1978) could not be studied because they occurred shortly after larger earthquakes elsewhere. The remaining earthquakes in the Tien Shan were too small to be analyzed using this technique. We estimated the strike and dip of the nodal planes and the rake for these 11 earthquakes with uncertainties of 5°-15° (see the appendix). In contrast, published first-motion fault plane

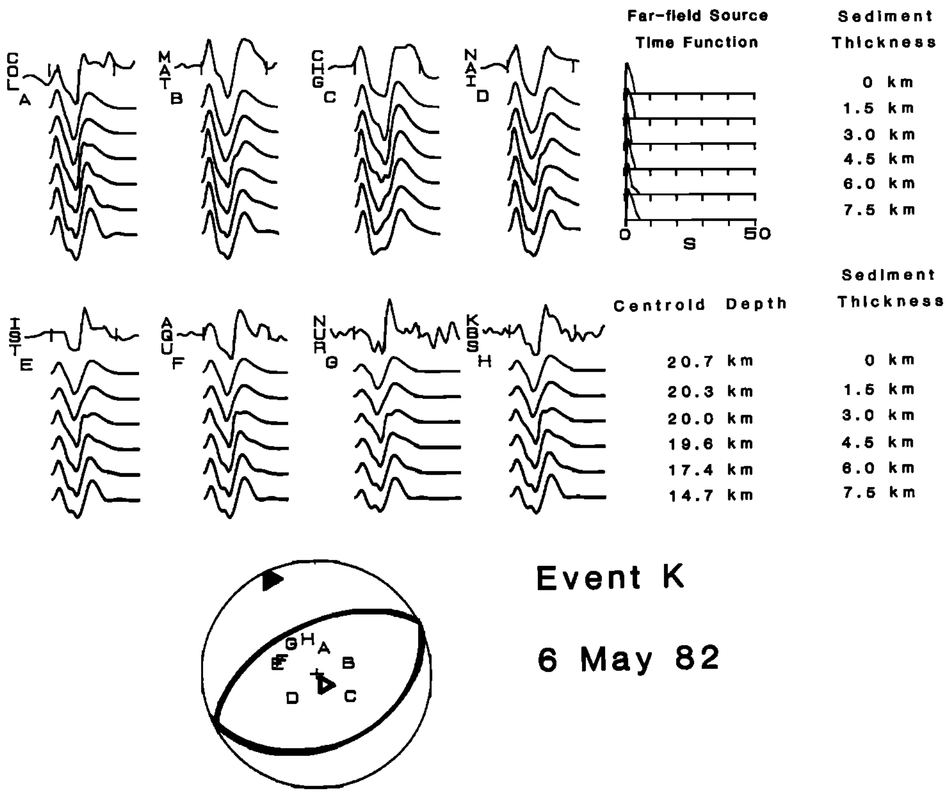

Fig. 2. Long-period P waveforms for earthquake K (May 6, 1982) recorded at eight WWSSN stations (top row) with synthetic seismograms illustrating the effects of varying the source velocity structure. The synthetic seismograms were generated using a crustal half-space overlain by a lower-velocity sediment layer (see Table 2). The waveforms for the half-space model (second row) do not match the sharp downturn following the direct P arrival. We explain this downturn as a reflection from the bottom of a sediment layer. The waveforms are fit best using a 4.5-km-thick sediment layer. The reflections from the base of the sediments and the free surface can be seen best at near-nodal stations (e.g., NUR and KBS) where the reflections from the sediment layer and the free surface appear as distinct downward pulses, producing a W-shaped trough. Also shown are the best fitting far-field source time function, centroid depth, and the lower hemisphere projection of the fault plane solution for each of the six velocity structures. The solid triangles mark the P axes; the open triangles mark the T axes. Note that changing the assumed velocity structure at the source has little effect on the inferred fault plane solution but the centroid depth decreases as the sediment layer is thickened.

solutions for the same earthquakes in the Tien Shan often disagree by as much as 45° in strike and rake angles because of the lack of data from local stations (compare Ni [1978] and Tapponnier and Molnar [1979]). Waveforms allow the centroid depths to be determined with uncertainties of only 3-7 km. Our results show that for these earthquakes the depths determined by the International Seismological Centre (ISC), using reported P wave arrival times and pP-P times, are often inaccurate by more than 30 km.

We digitized WWSSN long-period P and SH waveforms recorded at epicentral distances of 30°-86° for P waves and 30°-72° for SH waves. For these distance ranges the effects of upper mantle triplications and core phases are avoided; the long-period waveforms are most strongly influenced by the source mechanism and depth of the earthquake and the source and receiver velocity structures [Langston and Helmberger, 1975]. An inversion routine similar to that of Nabelek [1984, 1985] was used to determine the best fitting double-couple fault plane solution, far-field source time function, and centroid depth. The fault plane solution is specified by the strike and dip of one of the two nodal planes and the rake on that plane, following the convention Aki and Richards [1980, Figure 4.13]. We estimate typical uncertainties to be dip, ±5°; strike, ±10°; rake, ±15°; and centroid depth, 3 km plus 10% of the depth. In the appendix we discuss the assumptions made in modeling the seismograms and the uncertainties that result from those assumptions. In addition, we present waveforms for a range of source parameters for one deep (depth ≈ 40 km) and one shallow (depth ≈ 12 km) representative earthquake, so that readers can judge for themselves the uncertainties in the solutions.

Seismic Velocity Structure in the Source Region

The seismic velocity structure of the Tien Shan is poorly constrained due to the lack of

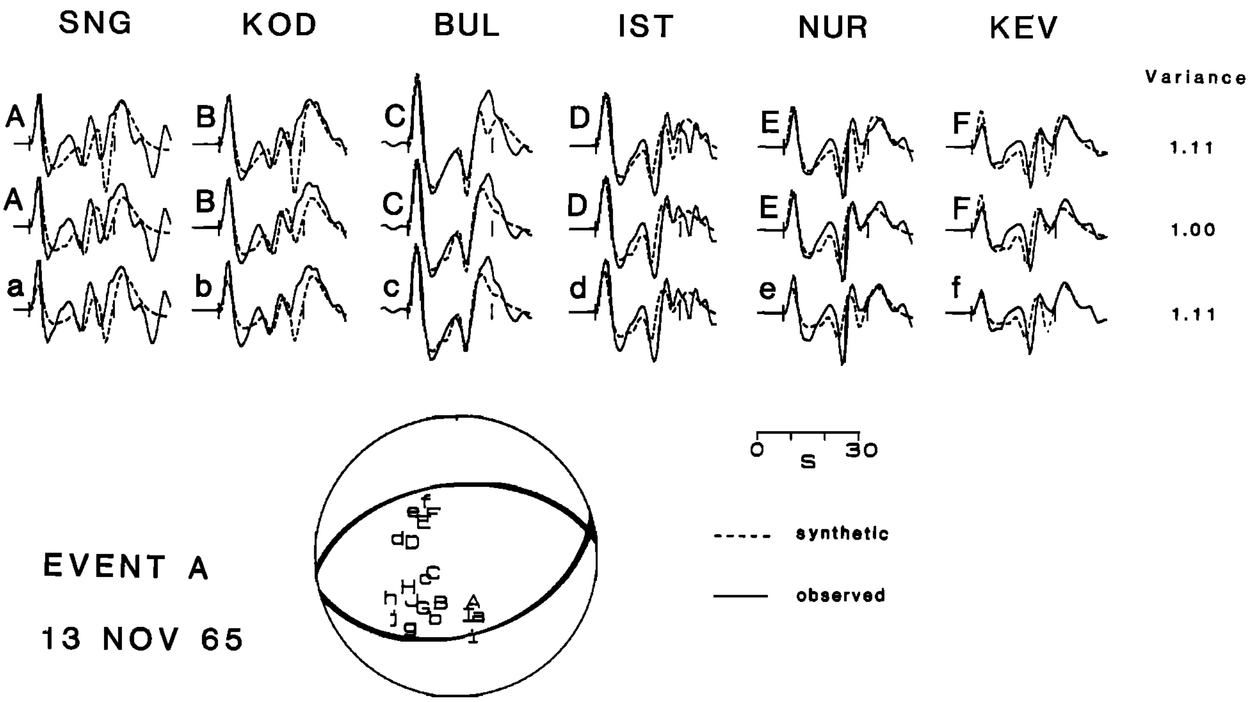

Fig. 3. Recorded waveforms (solid line) and synthetic (dashed line) seismograms for the earthquake A (November 13, 1965) for three assumed source velocity structures. The top row of seismograms shows the best fit solution using a half-space with v_p = 6.2 km/s. The second row shows the improved fit when a 12-km-thick low-velocity (v_p = 4.2 km/s) layer is included above the half-space. The third row shows the effect of putting the source in a mantle velocity layer (v_p = 8.0 km/s) beneath the sediment and crustal layers. On the lower hemisphere projection, lower case letters mark the stations for a mantle source, upper case letters mark the stations for a crustal source. When a mantle source velocity is used, the direct P (first upward pulse) amplitude is too small at those stations that fall close to the nodal planes (SNG, KOD, NUR, KEV) relative to that at stations far from the nodal planes (e.g., BUL and IST). Regional stations (Δ = 16°-21°) QUE (H), LAH (J), and NDI (G) recorded compressional first motions while SHL (I) recorded a dilatational first motion.

appropriate seismic refraction studies. For each earthquake the inversion routine was first run using a crustal half-space in the source region (v_p = 6.0-6.2 km/s, $v_s = v_p/\sqrt{3}$, density = 2700-2800 kg/m^3 with the larger values of v_p and density used for the deeper earthquakes). For four of the earthquakes (A, F, I, and K) there were clear phases on the observed seismograms which could not be explained using a half-space. To explain these phases and to study the dependence of the synthetic seismograms on the source velocity structure, we calculated seismograms for a variety of such structures. It is not possible to determine uniquely the source velocity structure using long-period seismograms. However, it is possible to recognize and discard inappropriate source velocity structures and thus decrease the mismatch between the synthetic and observed seismograms due to an unrealistic velocity structure. This in turn decreases the uncertainty in the inferred focal parameters.

For earthquake K shown in Figure 2 the amplitude and timing of the direct P and reflected phases could be matched using a crustal half-space, but an additional reflected phase is seen consistently before the pP phase. This phase is clearest at the European stations (AQU, NUR, and KBS) shown in Figure 2 where it causes a sharp dip after the small, nearly nodal direct P arrival (the upward phase starting at the tick mark). At NUR this phase and the pP phase that follows it form a W-shaped trough. We interpret this first negative polarity phase as a reflection from a boundary below the free surface. By adding a 4.5-km-thick layer (v_p = 3.0 km/s, v_s = 1.73 km/s, density = 2400 kg/m^3) the additional phase is matched well as a reflection from the base of this layer. Note that this change in velocity structure changed the inferred strike, dip, and rake of the fault plane solution by less than 1°, while the inferred depth decreased from 20.7 to 19.6 km.

The presence of sediments also affects the amplitude of the reflected phases. The Ürümqi earthquake of November 13, 1965 (event A), is deep enough that the reflected phases are clearly separated from the direct phases on the seismograms (Figures 3 and 6). For a crustal half-space (v_p = 6.2 km/s) the timing of the reflected phases is matched well, but their amplitudes relative to the direct P are not. As shown in the first row of seismograms in Figure 3, the mismatch is particularly large for sP, the sharp downward pulse that starts about 20 s after the direct P arrival. A 12-km-thick lower-velocity (v_p = 4.2 km/s) sedimentary layer over the half-

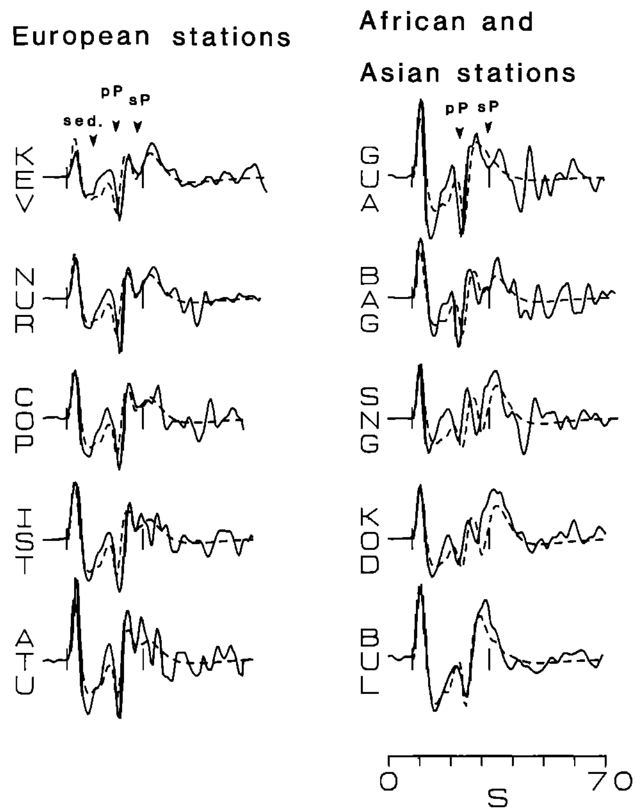

Fig. 4. Effects of azimuthal variations in the source velocity structure surrounding earthquake A (November 13, 1965). Solid lines represent the recorded waveform, and the dashed lines represent the best fitting synthetic seismograms. The reflected P waves which bounce off the sediment-basement contact (sed.) and the free surface (pP) are marked, as is the SV wave reflected from the free surface (sP). At the European stations to the northwest the reflected phases pP and sP arrive about 1 s late relative to those predicted by the synthetic seismograms. For Asian and African stations to the south of the epicenter the reflected phases arrive about 1 s early. We attribute this 2-s difference to the thick (>10 km) sediments of the Dzungarian Basin north of the epicenter.

space decreases the amplitude of the reflected phases and decreases the variance by about 10%.

Besides finding evidence for the presence of a thick section of sediments above the hypocenter, we can also test the possibility that this earthquake is in the mantle, by placing it in a half-space with v_p = 8.0 km/s, density = 3300 kg/m^3, beneath the sedimentary layer and a 30-km-thick crustal layer. The resulting increase in takeoff angles causes several of the stations (e.g., SNG, KOD, NUR, KEV) to fall closer to the nodal planes (Figure 3). At those stations the amplitude of the direct P phase for the best fit solution is too small. The increased misfit between seismograms caused by putting the source in the mantle suggests that the centroid is in the lower crust.

The P wave first motion recorded at SHL (Δ = 18.6°) is dilatational and apparently contradicts the evidence just presented (Figure 3). Specifically, SHL falls in the dilatational quadrant if a mantle source is assumed but in the compressional quadrant if a crustal source is assumed. However, in this distance range the actual takeoff angle of the first-arriving ray has a large uncertainty (5°-10°) because its turning point is in the uppermost mantle where the velocity structure is poorly known. Because of this uncertainty, we think that the waveforms provide more convincing evidence and conclude that the source was in the lower crust. As shown in Figure 3, the change in the assumed velocity structure does not significantly affect the best fit double-couple orientation. However, when a mantle source is assumed, the depth increases by 0.5 km and the seismic moment increases by 60%.

A systematic mismatch between some observed waveforms and their corresponding synthetic seismograms generated using a plane-layered source structure indicates that the source velocity structure varies with azimuth. For example, a close look at the synthetic and the recorded seismograms for the November 13, 1965, earthquake (Figure 4) reveals that the interval between the P and pP phases is consistently about 2 s less at southern Asian and African stations than at European stations (Figure 4). The epicenter for this event is near Ürümqi, near the southern edge of the Dzungarian Basin, which reputedly contains up to 11 km of sediments [Terman et al., 1967]. For a focal depth of 44 km the bounce points for pP and sP are between 20 and 30 km from the epicenter. Consequently, pP and sP ray paths to Europe will pass through some of these sediments, while ray paths to southern

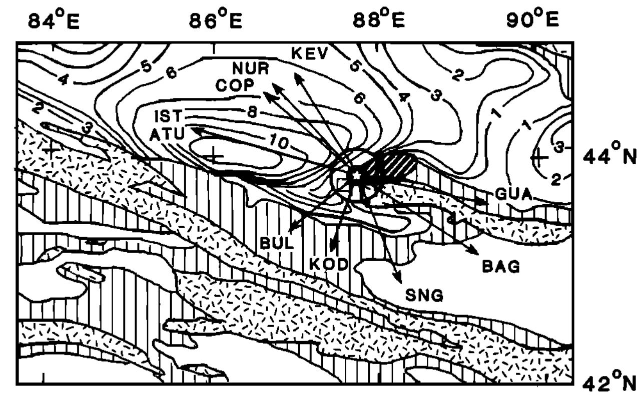

Fig. 5. Epicentral region earthquake A of November 13, 1965. The unshaded regions are basins. Isopachs of Mesozoic and Tertiary sediment thickness in the Dzungarian Basin are marked in kilometers [Terman et al., 1967]. Paleozoic sediment is indicated by vertical lines, and crystalline basement is cross-hatched. Star marks the ISC epicenter. The hatched oval northeast of Ürümqi is the area of maximum intensity (Modified Mercali 8) according to the State Seismology Bureau of China [1979]. The circle represents the locus of bounce points for pP. Arrows show the directions of ray-paths to European, African, and Asian stations shown in Figure 4. The reflected phases at the European stations are delayed 2.0-2.5 s, with respect to those of the Asian stations, probably by transmission through the thick sediments of the Dzungarian Basin.

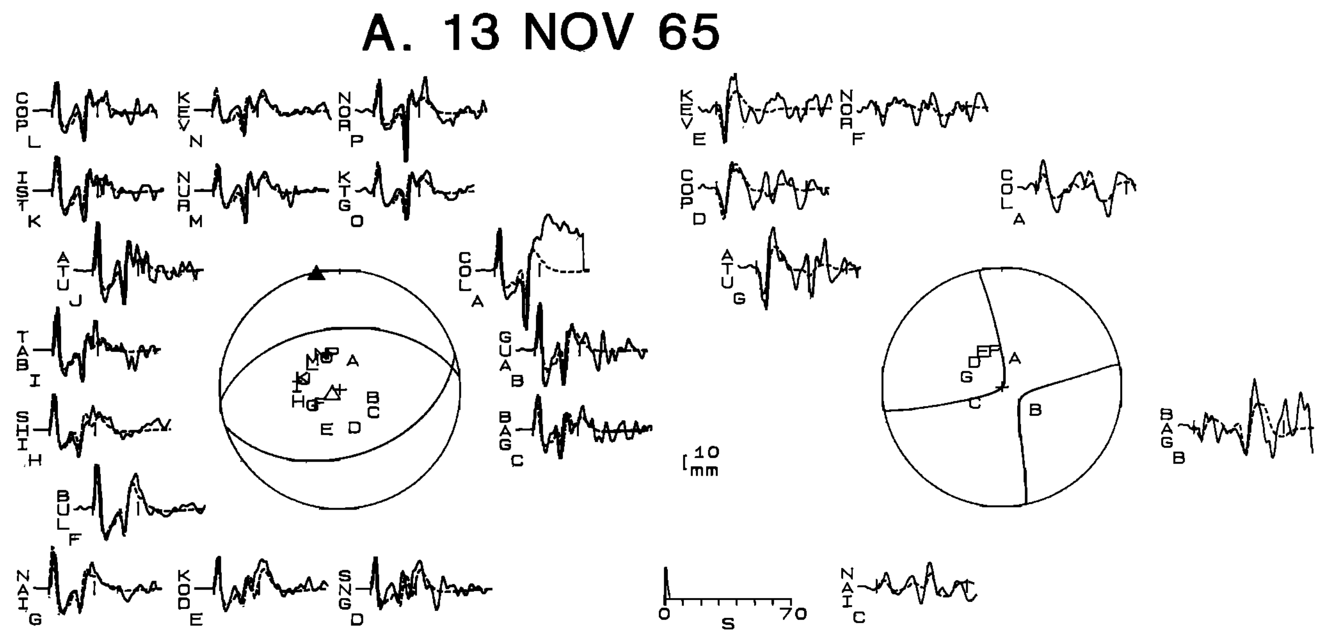

Fig. 6. Fault plane solution and waveforms for earthquake A (November 13, 1965). Recorded (solid) and synthetic (dashed) seismograms are shown with tick marks enclosing the part of the seismogram used in the inversion. The lower hemisphere plots show the locations of the stations and the nodal surfaces on the focal sphere (P on the left, SH on the right). Solid triangle marks the P axis, and open triangle marks the T axis. The normalized source time function is shown on the time scale axis. Seismograms are scaled to a common epicentral distance (Δ = 40°) and instrument magnification (3000×). The amplitude scale corresponds to waveforms that would be observed on such an instrument at such a distance. The source velocity structure is given in Table 2. Depth phases indicate a centroid depth of 44 ± 7 km.

Asia and Africa will travel through the basement rock exposed in the Tien Shan range, as illustrated in Figure 5. The observed 2.0- to 2.5-s delay of the pP phase at European stations could be explained if it traversed 13-16 km of sedimentary rock with an average v_p = 4.2 km/s instead of crystalline rock (assumed v_p = 6.2 km/s). Synthetic seismograms in Figures 4 and 6 were generated using a crustal half-space overlain by a 12-km-thick low-velocity layer.

Although the real source velocity structure is different from the assumed plane-layered velocity structure, and these differences will lead to some mismatch between the synthetic and the observed seismograms, it is the orientation of the nodal planes and the centroid depth that have the largest effect on the waveforms. Consequently, the best fit fault plane solution varies little if the source velocity structure is changed (Figures 2 and 3).

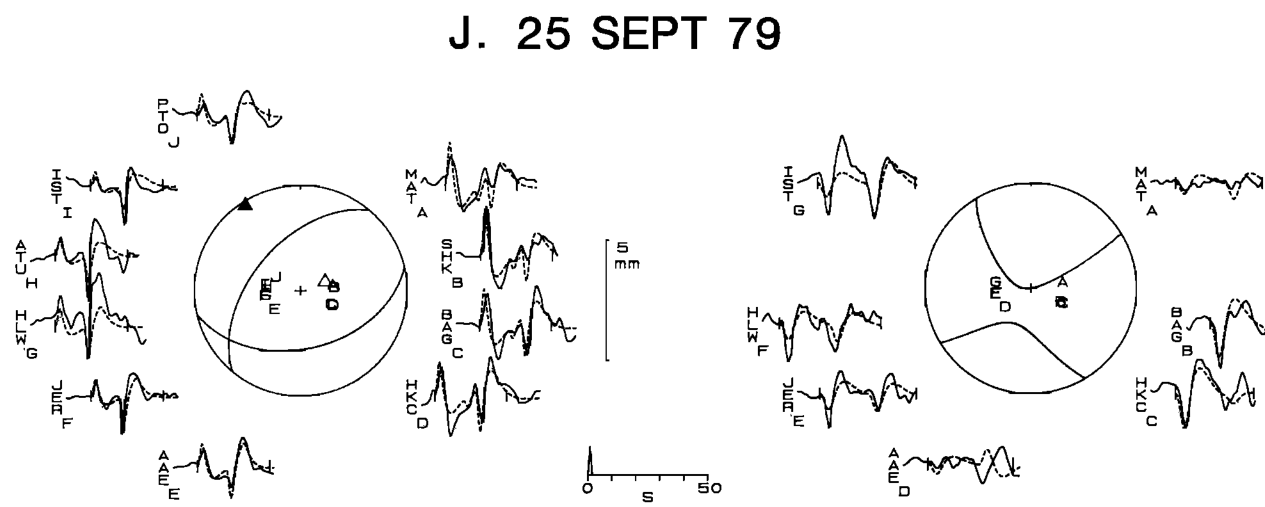

Fig. 7. Fault plane solution and waveforms for earthquake J (September 25, 1979). Format as in Figure 6. The centroid depth is 40 ± 7 km.

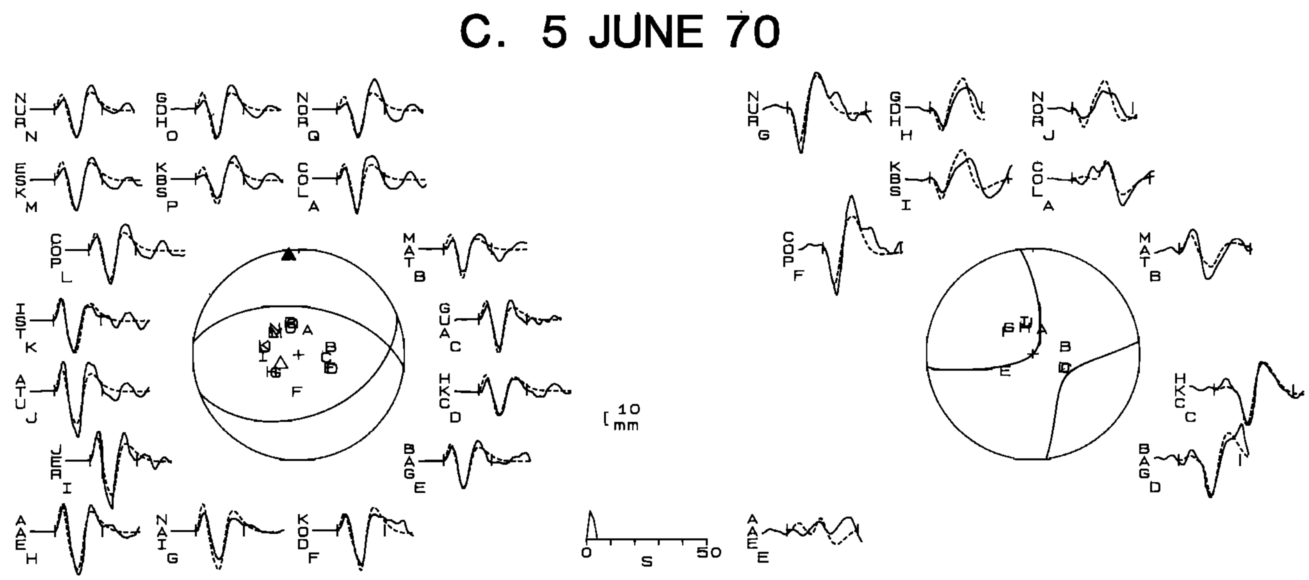

Fig. 8. Fault plane solution and waveforms for earthquake C (June 5, 1970). Format as in Figure 6.

Results

Earthquakes in the northern Tien Shan. Five of the earthquakes studied occurred at or north of the northern edge of the Tien Shan (earthquakes A, C, E, G, J; Figure 1). All five are characterized by thrust or oblique thrust mechanisms with north-northeast to north-northwest trending P axes. For all but one earthquake the nodal planes dip between 40° and 55° (Figures 6-10). The source durations are short (<5 s), and the centroid depths range from 15 to 44 km.

The deepest and largest earthquake studied occurred ≈50 km northeast of Ürümqi in the Chinese Tien Shan on November 13, 1965 (earthquake A, Figures 1 and 6, Table 1). The ISC epicenter and the Chinese isoseismal maps [State Seismology Bureau of China, 1979] indicate that this earthquake occurred under the western end of the Bogda Ula range (Figure 5). The P and SH waveforms indicate nearly pure thrust faulting with moderately dipping nodal planes striking just north of east (Figure 6). The strikes of the nodal planes roughly parallel both the northern edge of the range and the long axis of the elliptical zone of maximum intensity (Modified Mercali 8) (Figure 5). Which of the nodal planes is the fault plane could not be determined from the waveforms. The centroid depth of 44 ± 7 km and short source time function (<3 s) indicate that faulting did not extend into

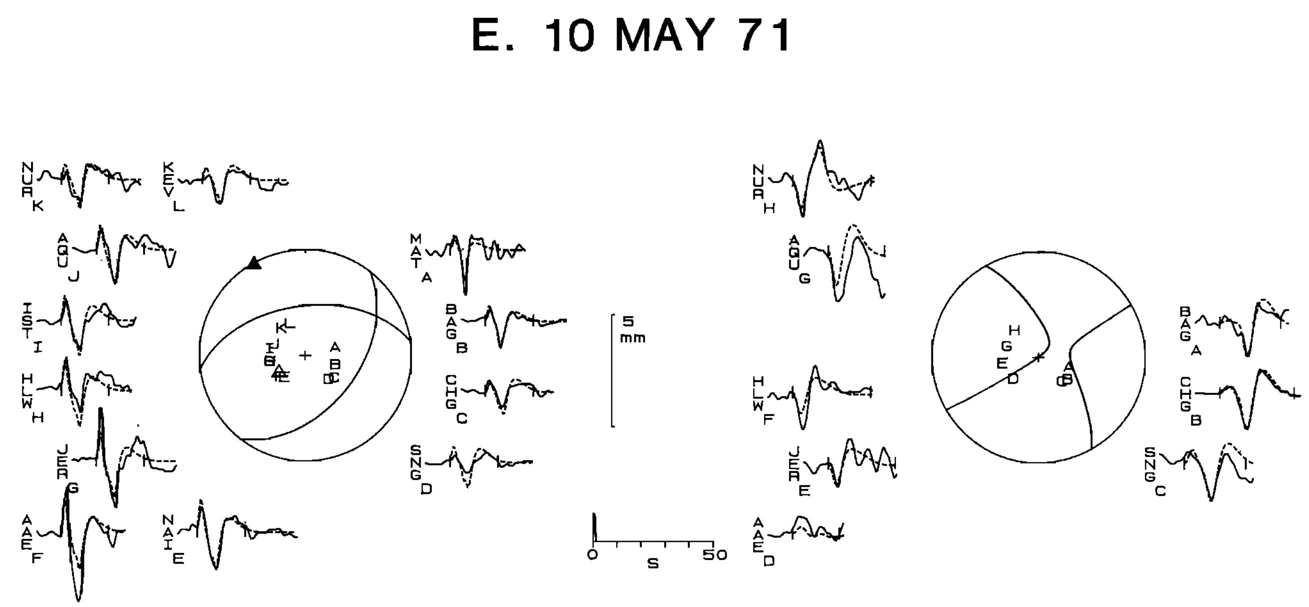

Fig. 9. Fault plane solution and waveforms for earthquake E (May 10, 1971). Format as in Figure 6.

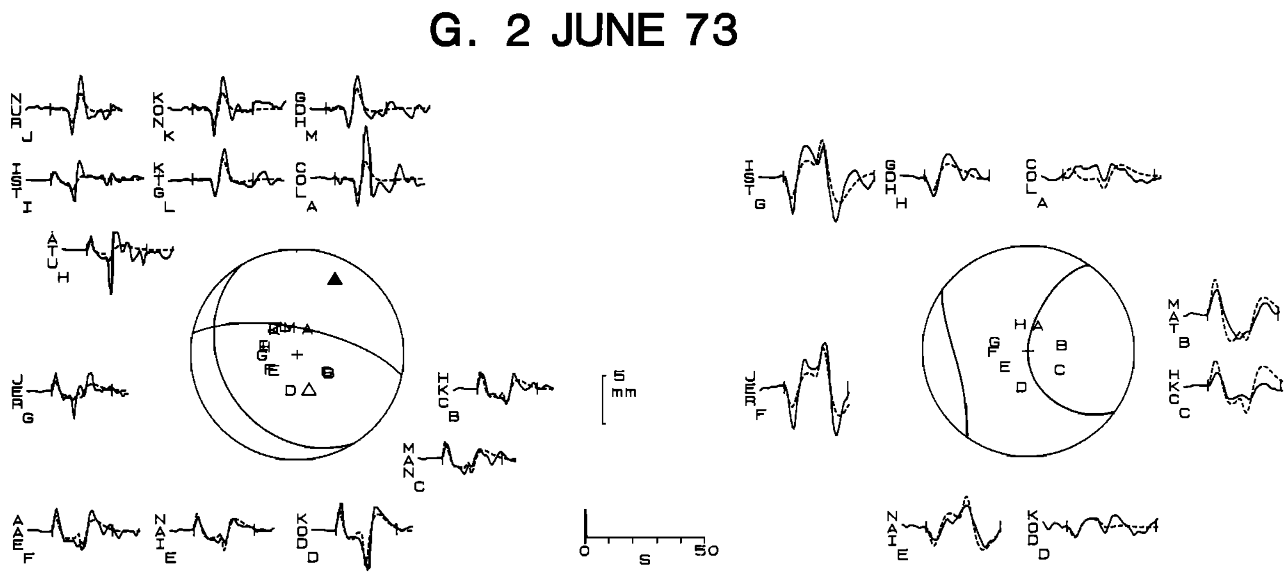

Fig. 10. Fault plane solution and waveforms for earthquake G (June 2, 1973). Format as in Figure 6.

TABLE 1. Focal Mechanisms for 11 Tien Shan Earthquakes

	Date	Origin Time (UT)	Epicenter (ISC) Latitude	Epicenter (ISC) Longitude	Focal Mechanism Strike	Focal Mechanism Dip	Focal Mechanism Slip	Moment, 10^{17} N m	Source Duration, seconds	Centroid Depth, km
A	Nov. 13, 1965	0433:50.6	43.87° N	87.74° E	72° 264°	43° 48°	81° 98°	37	2.4	44
B	Feb. 11, 1969	2208:51.0	41.42° N	79.24° E	65° 253°	41° 49°	83° 96°	20	6.9	10
C	June 5, 1970	0453:07.4	42.48° N	78.71° E	69° 277°	41° 53°	68° 108°	31	3.8	17
D	March 23, 1971	2047:16.0	41.42° N	79.20° E	73° 248°	46° 44°	93° 87°	5.9	7.0	11
E	May 10, 1971	1451:45.0	42.85° N	71.29° E	37° 262°	48° 51°	57° 122°	1.3	1.3	15
F	April 9, 1972	0410:48.9	42.09° N	84.58° E	100° 279°	49° 41°	90° 90°	1.3	1.0	13
G	June 2, 1973	2357:02.4	44.14° N	83.60° E	148° 282°	28° 70°	133° 70°	2.1	0.8	26
H	Jan. 31, 1977	1426:15.1	40.11° N	70.86° E	81° 249°	40° 51°	100° 82°	5.2	1.0	12
I	March 29, 1979	0201:32.1	41.95° N	83.38° E	71° 258°	53° 38°	86° 96°	2.3	1.3	13
J	Sept. 25, 1979	1305:54.5	45.09° N	76.96° E	77° 220°	44° 52°	119° 65°	1.7	2.0	40
K	May 6, 1982	1542:22.2	40.15° N	71.54° E	70° 244°	36° 54°	95° 86°	2.0	3.6	20

Estimated uncertainties: strike ±10°, dip ± 5°, rake ±15°, and depth ± 3-7 km.

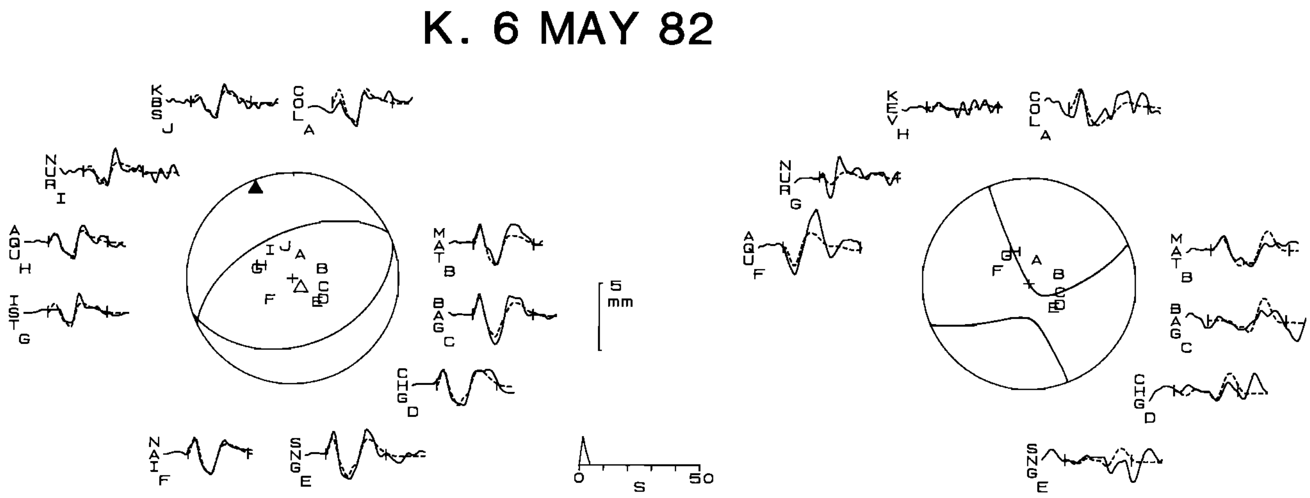

Fig. 11. Fault plane solution and waveforms for earthquake K (May 6, 1982). Format as in Figure 6.

the upper crust, and we are not aware of any reports of surface rupture. It is thus difficult to link the earthquake to any particular fault, although we suspect that the earthquake occurred on the downward continuation of one of the south dipping thrust faults that runs along the north side of the range.

This earthquake is notable because it is surprisingly deep for a crustal intracontinental earthquake. Both Chen and Molnar [1977] and Vilkas [1982] noted that the focal depth of this event was >40 km. There are no published refraction profiles from the Chinese Tien Shan and little gravity data, so the crustal thickness beneath the Bogda Ula is not constrained well. Zhang et al. [1984] published a map of crustal thickness for China showing the Moho at a depth of 46-50 km in the Ürümqi area. The average elevation in the source region of ≈3 km would imply a Moho depth of ≈50 km if the region is isostatically compensated. Hence the centroid depth of 44 ± 7 km places the earthquake in the lower crust, although it may have extended into the mantle. As discussed above, waveforms are

TABLE 2. Source Velocity Structures Used to Generate Synthetic Waveforms

	Event	Layer Thickness, km	Seismic Velocity, km/s v_p	Seismic Velocity, km/s v_s	Density, kg/m³
A	Nov. 13, 1965	12	4.20	2.40	2500
		half-space	6.20	3.60	2800
B	Feb. 11, 1969	half-space	6.00	3.46	2700
C	June 5, 1970	half-space	6.10	3.50	2800
D	March 23, 1971	half-space	6.00	3.46	2700
E	May 10, 1971	half-space	6.00	3.46	2800
F	April 9, 1972	7	4.00	2.30	2500
		half-space	6.20	3.60	2800
G	June 2, 1973	half-space	6.10	3.50	2800
H	Jan. 31, 1977	half-space	6.00	3.50	2700
I	March 29, 1979	7	4.00	2.30	2500
		half-space	6.00	3.46	2700
J	Sept. 25, 1979	half-space	6.05	3.50	2800
K	May 6, 1982	4.5	3.00	1.73	2400
		half-space	6.10	3.50	2800

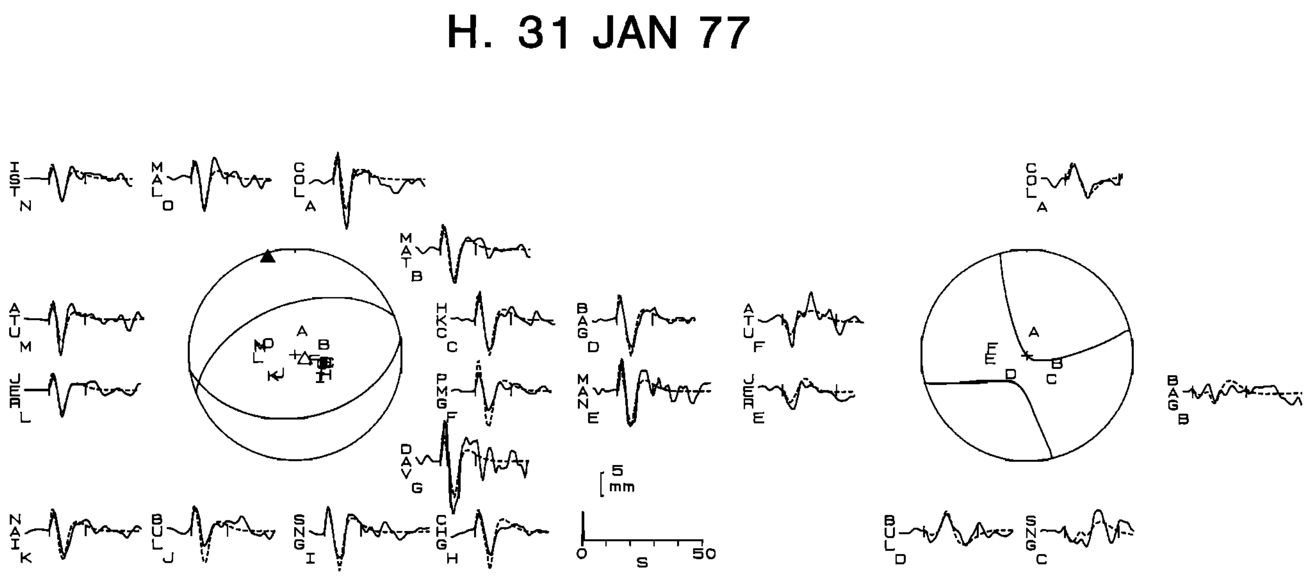

Fig. 12. Fault plane solution and waveforms for earthquake H (January 31, 1977). Format as in Figure 6.

matched best for a crustal velocity in the source region.

Earthquake J, on September 25, 1979, was also unusually deep (40 ± 7 km) and indicates oblique thrust faulting well north of the main part of the Tien Shan (Figures 7 and 19). A Soviet seismic refraction profile, east of the epicenter, was interpreted as showing a 48-km-thick crust consisting of an 11-km-thick layer (v_p = 5.5 km/s) overlying a higher-velocity (v_p = 6.3 km/s) layer [Gamburtsev et al., 1955; Vol'vovskii and Vol'vovskii, 1975]. We approximated the crust with a half-space (v_p = 6.2 km/s), but the quoted uncertainty in the centroid depth reflects the range of plausible velocity structures (average v_p = 5.6-6.8 km/s). This ±10% range in average seismic velocity for the Tien Shan leads to a ±10% uncertainty in the depth in addition to the ±3 km uncertainty demonstrated in the appendix. Again the centroid depth indicates that faulting occurred in the lower crust.

The centroid depths of the remaining three earthquakes along the northern edge of the Tien Shan (earthquakes C, E, and G) are midcrustal (15-26 km). All three events reflect thrust or oblique thrust faulting with north-northwest and north-northeast trending P axes (Figures 1 and 8-10).

Earthquakes in the Fergana Basin. Earthquakes H and K occurred beneath the southern edge of the Fergana Basin, which lies in the western Tien Shan between the Chatkal range on the north and the Alay range on the south (Figure 1). The elevations in the basin are ≈1000 m, but peaks of the ranges flanking it reach over 4500 m. East-west striking thrust faults bound the basin, which in places contains more than 9 km of sediments [Krestnikov, 1962; Terman et al., 1967; Vol'vovskii and Vol'vovskii, 1975]. Both events are characterized by nearly pure thrust mechanisms with moderately dipping nodal planes (35°-55°) and north-northwest trending P axes. Presumably, the nodal planes that dip south beneath the mountains are the fault planes.

The epicenter published by the ISC for event K is at the foot of the mountains south of the basin. The Soviet seismological network, with stations in the Fergana Basin, located the earthquake approximately 25 km farther to the north and beneath the basin at a depth of 20 km. We found the centroid depth to be 20 ± 5 km. The waveforms for this earthquake could not be matched well using a half-space, particularly for stations to the northwest where a phase prior to pP is clearly visible (Figures 2 and 11). Using a 4.5-km-thick low-velocity sedimentary layer over a half-space produced synthetic seismograms that matched this feature better (Table 2). We thus infer that there are several kilometers of sediments within a few tens of kilometers of the thrust faults along the southern edge of the Fergana Basin. This requires that the crystalline rocks of the Tien Shan have been uplifted several kilometers along the range-bounding thrust faults and juxtaposed against the thick sediments of the basin.

A second, shallower earthquake (H) occurred approximately 60 km west of event K, along the northern edge of the Alay range south of the Fergana Basin. The waveforms were matched (Figure 12) using a half-space (Table 2), and the centroid depth was found to be 12 ± 4 km. Because the earthquake was rather shallow, the depth phases interfere, and a reflection from the base of a sediment layer, if present, would be difficult to see. Presumably, both of these earthquakes occurred along south dipping thrust faults on which the mountains to the south are thrust northward over the sediments of the basin.

Earthquakes along the southern edge of the Tien Shan. Four of the earthquakes studied occurred along the southern edge of the Chinese Tien Shan (Figure 1). All four occurred at depths of less than 15 km on moderately dipping (40°-50°) thrust faults. The P axes indicate roughly north-south shortening. Along the southern edge of the Tien Shan the bedrock of the mountains is thrust southward over the alluvium of the Tarim Basin, so that the nodal planes

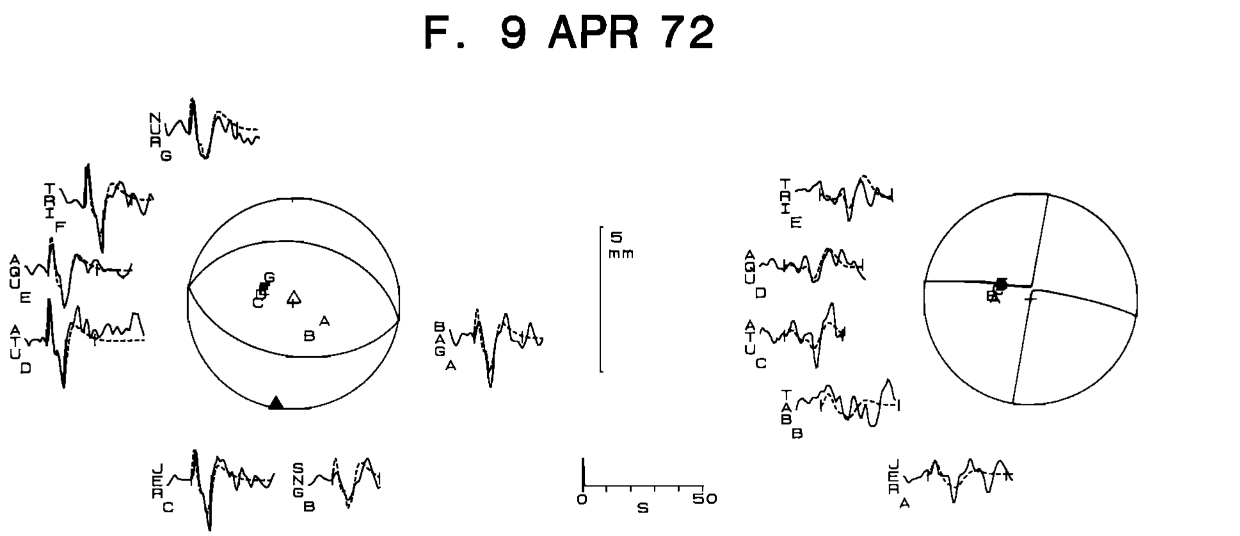

Fig. 13. Fault plane solution and waveforms for earthquake F (April 9, 1972). Format as in Figure 6.

dipping north beneath the mountains are probably the fault planes.

Earthquakes F and I both are characterized by pure thrust faulting with north trending P axes. Both events are relatively small (m_b = 5.8) with sharp, uncomplicated waveforms and shallow centroid depths (13 ± 4 km). In neither case could the waveforms be matched well using a half-space. On records from European stations (e.g., ATU and AQU), there is a small phase after the direct P but before the large sP phase (Figures 13 and 14). This phase causes the inflection seen in the downswing following the sharp up of the P arrival. It is too early to be the pP phase; the waveforms are not matched well using only a half-space. A two-layered structure with a 7.0-km-thick lower-velocity layer over a half-space (see Table 2) can produce such a phase with the correct timing and amplitude. The earthquakes occurred along the northern edge of the Kucha Basin, which reputedly contains as much as 9 km of sediments, although only 3 km of sediments are shown beneath the epicentral region by Terman et al. [1967]. However, in this area, their map is based upon sparse data, and apparently, they assumed that the sediments do not extend beneath the thrust faults of the Tien Shan. The waveforms suggest that there are several kilometers of sediments in the region, which may indicate the underthrusting of Tarim Basin sediments.

The remaining two earthquakes (B and D) are among the largest in a swarm of earthquakes along the southern edge of the Chinese Tien Shan near the border between China and the Soviet Union. A third large event occurred in the same region, also on March 23, 1971, but could not be studied due to an earlier, large earthquake elsewhere.

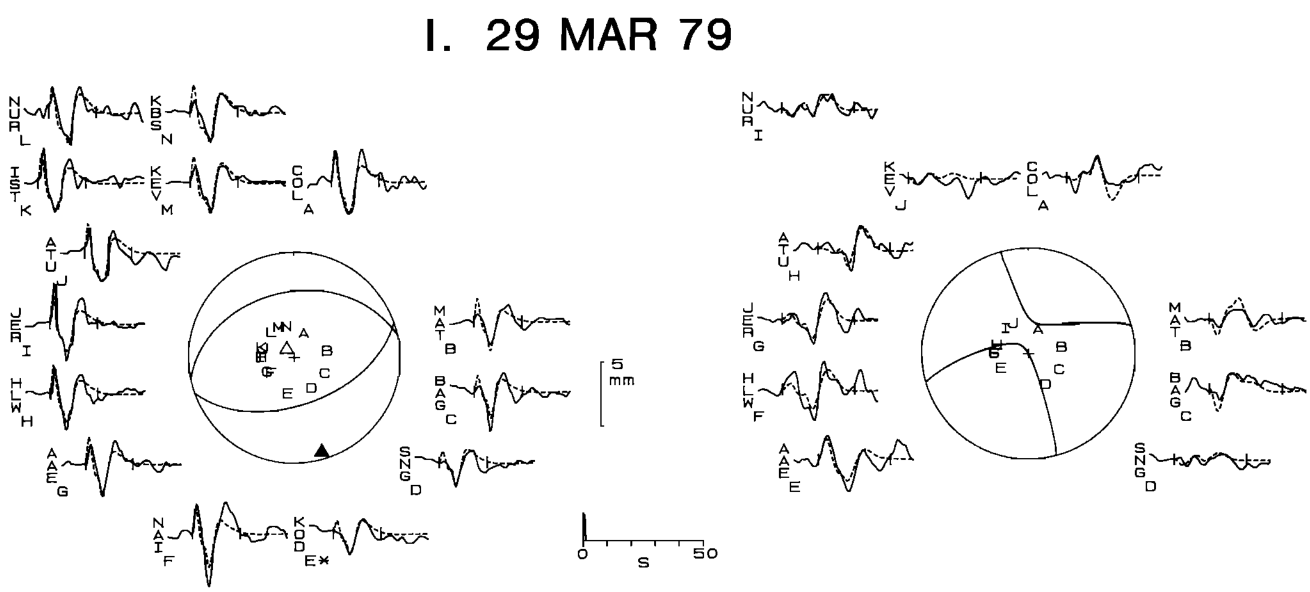

Fig. 14. Fault plane solution and waveforms for earthquake I (March 29, 1979). Format as in Figure 6.

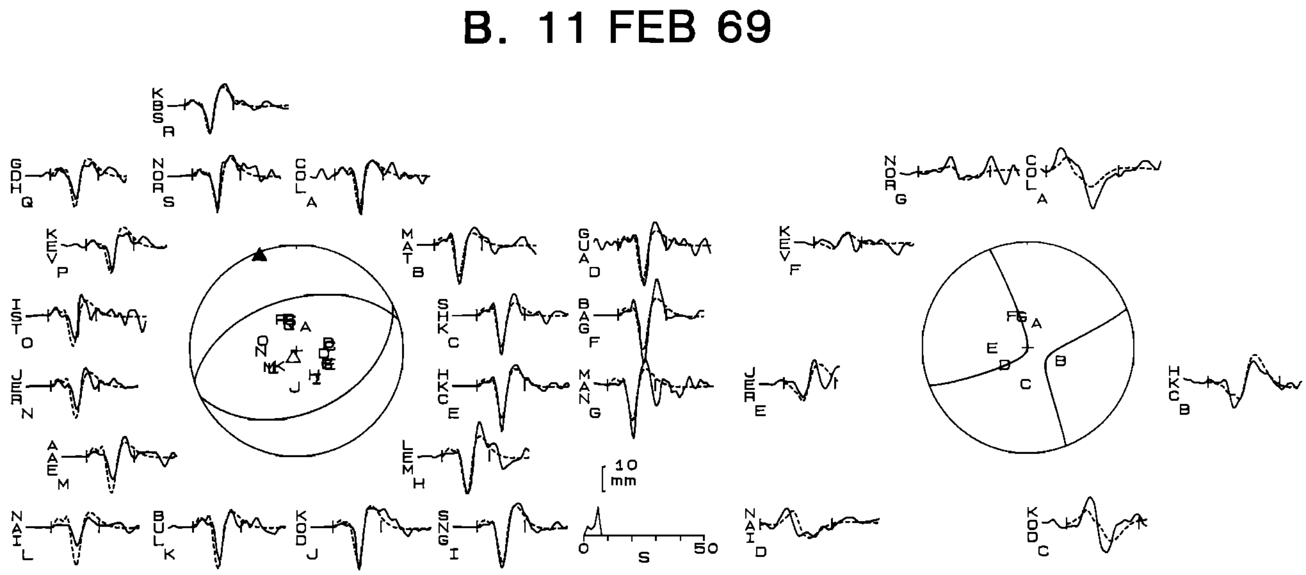

Fig. 15. Fault plane solution and waveforms for earthquake B (February 11, 1969). Format as in Figure 6.

The events studied were similar in magnitude (m_b = 5.8), and the similar fault plane solutions indicate thrusting to the south-southeast on moderately dipping (39°-54°) fault planes (Figures 15 and 16).

Conclusions

The focal mechanisms of all 11 earthquakes studied include large thrust components and indicate north-northwest to north-northeast shortening. With one exception (earthquake G) the nodal planes are moderately dipping (35°-55°) to the north and south. These events appear to have occurred on range-bounding faults that dip beneath the mountains, with the basement being thrust over the sediments of the basins flanking the ranges. For four earthquakes (A, F, I, and K) the waveforms contain phases that cannot be explained by a simple half-space velocity model but that can be explained as reflections from the base of a thick sediment layer above the earthquake. Thus they suggest that there may be several kilometers of sediments thrust beneath the mountains that bound the Dzungarian, Fergana, and Kucha basins.

The centroid depths of these events range from 26-44 km for the three northernmost earthquakes to 10-13 km for those along the southern edge of the Tien Shan. These depths require that basement be involved in the shortening occurring in the Tien Shan. Two of the earthquakes (A and J) are unusually deep (≥40 km) for intracontinental earthquakes and probably occurred in the lowermost crust.

It is instructive to compare the Tien Shan to

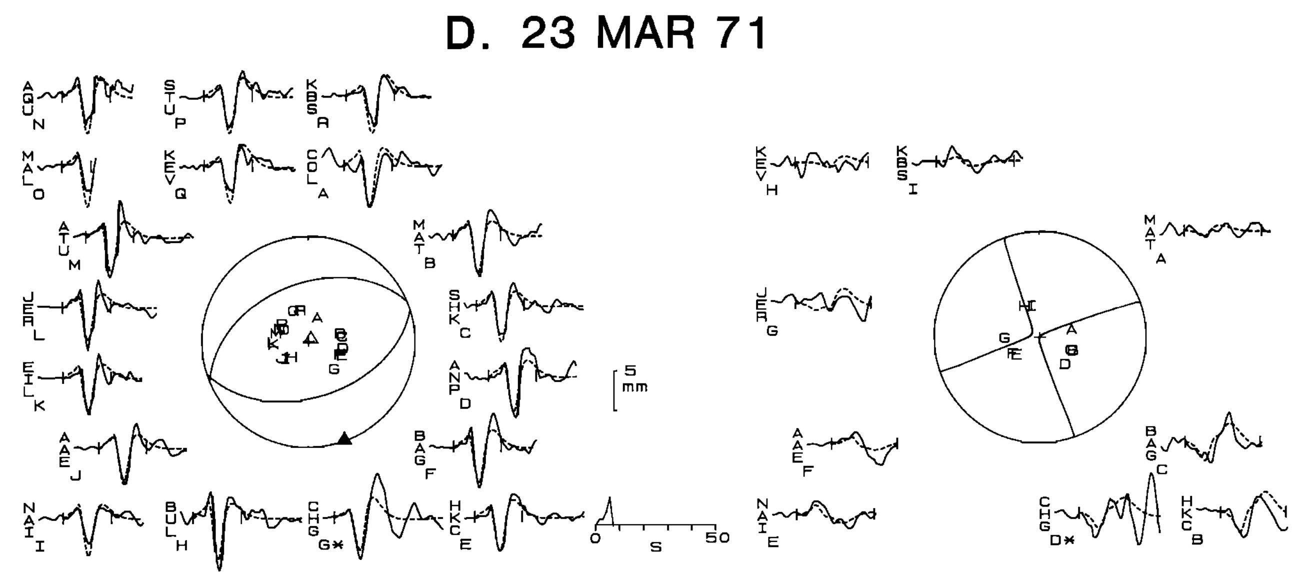

Fig. 16. Fault plane solution and waveforms for earthquake D (March 23, 1971). Format as in Figure 6. The seismograms for CHG (Δ = 28°) were not used in the inversion.

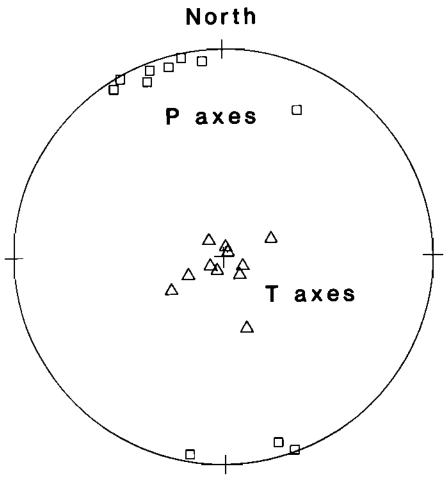

Fig. 17. Lower hemisphere equal-area projection of the P axes (squares) and T axes (triangles) of the earthquakes studied.

TABLE 3. Orientations of P and T Axes

	Date	P Axis		T Axis	
		Trend	Plunge	Trend	Plunge
A	Nov. 13, 1965	348.5°	2.5°	235.0°	83.6°
B	Feb. 11, 1969	339.0°	4.2°	205.0°	84.0°
C	June 5, 1970	354.2°	6.0°	242.0°	74.4°
D	March 23, 1971	160.2°	1.1°	44.2°	87.4°
E	May 10, 1971	330.4°	1.6°	237.0°	65.6°
F	April 9, 1972	190.0°	4.0°	12.3°	86.0°
G	June 2, 1973	27.0°	22.2°	162.4°	60.2°
H	Jan. 31, 1977	344.4°	5.6°	116.3°	81.6°
I	March 29, 1979	163.9°	7.6°	318.0°	81.5°
J	Sept. 25, 1979	327.3°	4.5°	69.8°	70.0°
K	May 6, 1982	337.0°	9.2°	138.7°	80.4°

other zones of intercontinental deformation far from plate margins. Are there other regions where shortening has occurred along moderately dipping thrust faults that involve basement and extend to depths of ≥40 km? One analog is in the Rocky Mountains of Colorado, Wyoming, and Utah where shortening in the late Cretaceous was accommodated by thrusting along faults like the Wind River Thrust, which dips 35°-45° and extends from the surface to depths of at least 30 km [Smithson et al., 1980]. During the Laramide orogeny, crustal shortening produced block uplifts similar to those in the Tien Shan.

The style of deformation in the Tien Shan and in the Rockies is not the only similarity. In both regions, crustal shortening has occurred thousands of kilometers from the plate margin. The consistent, north-south directions of the P axes suggest that the shortening seen in the Tien Shan is probably due to the collision of India with Eurasia ≈1500 km to the south [Tapponnier and Molnar, 1979]. The trends of the P axes for these earthquakes have been determined to within 10° (Figure 17 and Table 3) and are in accord with the orientations of maximum compressive stress predicted both by Tapponnier and Molnar's [1976] application of slip-line field theory to describe the deformation of Asia and by England and Houseman's [1985, 1986] calculations for a thin viscous sheet.

The east-west shortening in the Laramide Rockies is thought to be driven by subduction of the Farallon plate beneath the western edge of North America. To link the uplift of the Rockies with the subduction going on more than 1000 km to the west, some workers [e.g. Bird, 1984;

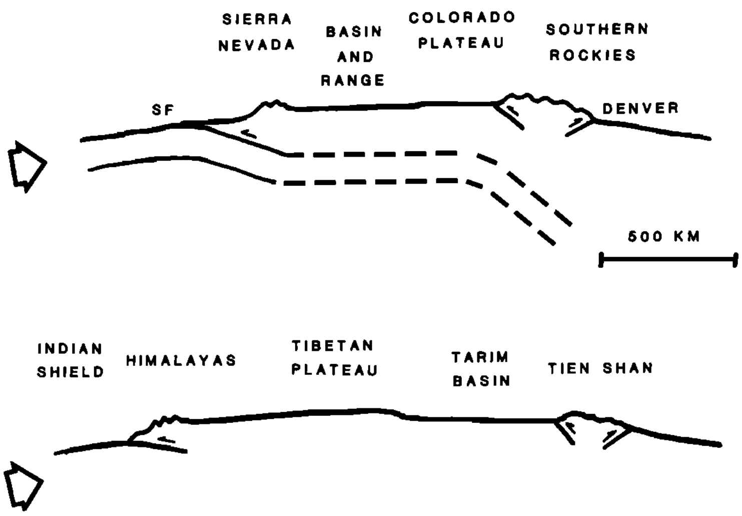

Fig. 18. Cartoon illustrating the similarities of tectonic setting and styles of deformation between the intracontinental thrusting in the Tien Shan and the Laramide thrusting in Wyoming, Utah, and Colorado during the Cretaceous period. In both cases shortening has occurred more than 1000 km from the plate margin where subduction occurred. Several workers have suggested that the Laramide thrusting was linked to the subduction of the Farallon plate beneath California by horizontal subduction. However, shortening is occurring in the Tien Shan today even farther from a plate margin, and there is no evidence of a horizontal slab beneath Tibet and the Tarim Basin.

Burchfiel and Davis, 1975; Dickinson and Snyder, 1978; Engebretson et al., 1984] have suggested that the subducting Farallon plate did not sink into the asthenosphere under California but instead moved horizontally under western North America, finally sinking into the asthenosphere beneath the Rockies (Figure 18). The shortening occurring today in the Tien Shan seems to be due to the collision of India with Eurasia, yet there appears to be no horizontal slab linking the two. If a slab were moving horizontally beneath Tibet and the Tarim Basin, we would expect to see Tertiary volcanism and numerous intermediate depth earthquakes there. However, there are very few outcrops of Tertiary volcanic rocks and very little seismicity in the Tarim Basin. Apparently, subduction of a horizontal slab is not required to cause the uplift of the Tien Shan. Although this analogy cannot prove that the Rockies are not related to horizontal subduction, it does show that it is not necessary to explain the Laramide shortening that occurred there.

Appendix: Uncertainties in Strike, Dip, and Rake Angles of Fault Plane Solutions

Several approximations to the real earth must be made in generating the synthetic seismograms, and each contributes to a misfit of the observed and synthetic seismograms that translates into an uncertainty in the parameters being estimated. Here we discuss these approximations and attempt to evaluate their effect on the solution.

Assumptions required to generate the synthetic seismograms include the instrument response, the attenuation operator, and the source and receiver velocity structure. With the exception of the source velocity structure, which is discussed above, these fixed parameters are known fairly well, and regardless, the synthetic waveforms change little if they are varied within

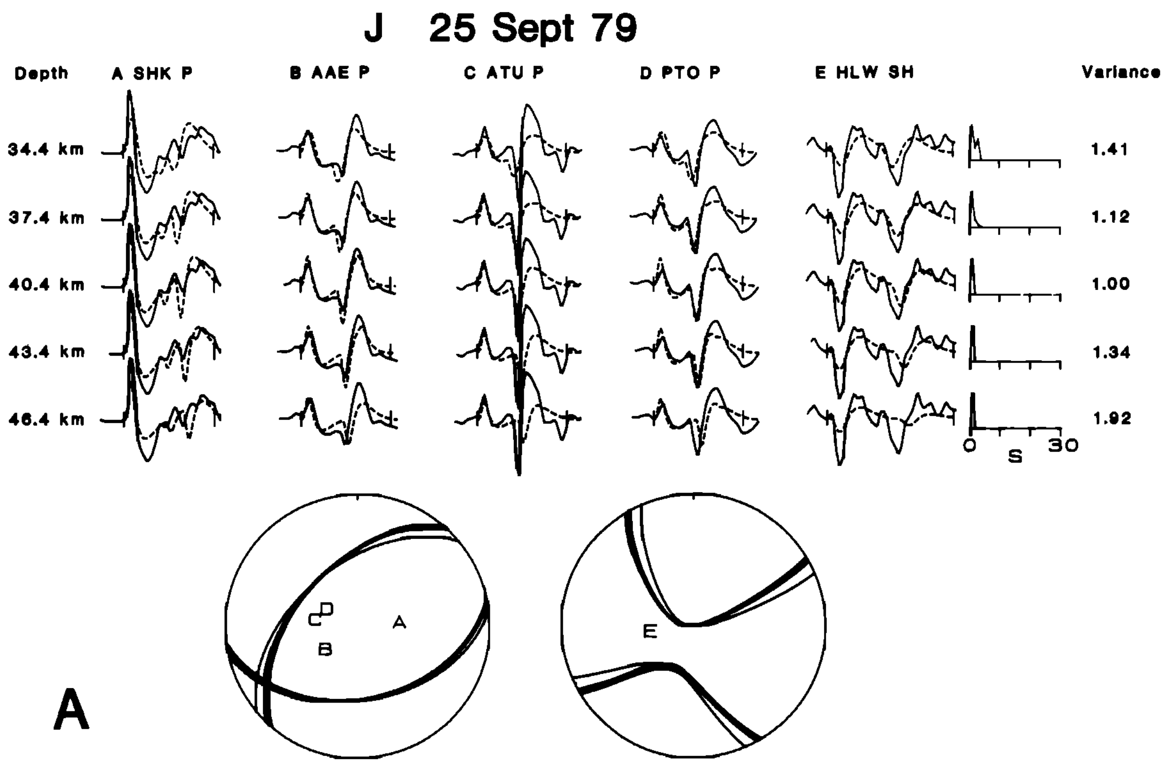

Fig. 19. Waveforms illustrating the uncertainties in parameters for the best fitting focal mechanism for earthquake J of September 25, 1979. (a) Best fitting solutions computed for each of five centroid depths. Observed (solid) and synthetic (dashed) waveforms from only diagnostic stations are shown (Figure 7 shows all waveforms used in the inversion). The time scale and source time function are shown on the right. The nodal surfaces and the positions of the stations are shown on a lower hemisphere projections of the focal sphere (P on left, SH on right). The best fit solution at a centroid depth at 40.4 km is shown by the middle row of seismograms. When the centroid depth is fixed above or below the best fitting depth, the reflected phases are not matched and the normalized variance increases. For a given source velocity structure, the centroid depth can be constrained in this way to within 3 km. Note that the focal mechanism changes very little as the depth is varied. (b) Similar diagrams in which the strike of the northwest dipping nodal plane is varied. Note that the middle two rows of seismograms are for the best fit solution with a strike of 220°. The SH waveforms in particular constrain the strike within 10°. (c) Similar diagrams showing how the dip can be constrained within 5°. Again the middle row(s) are for the best fit solution. (SH nodal surfaces are only shown for the best-fit solution.) (d) Similar diagrams showing how the slip can be constrained within 15°.

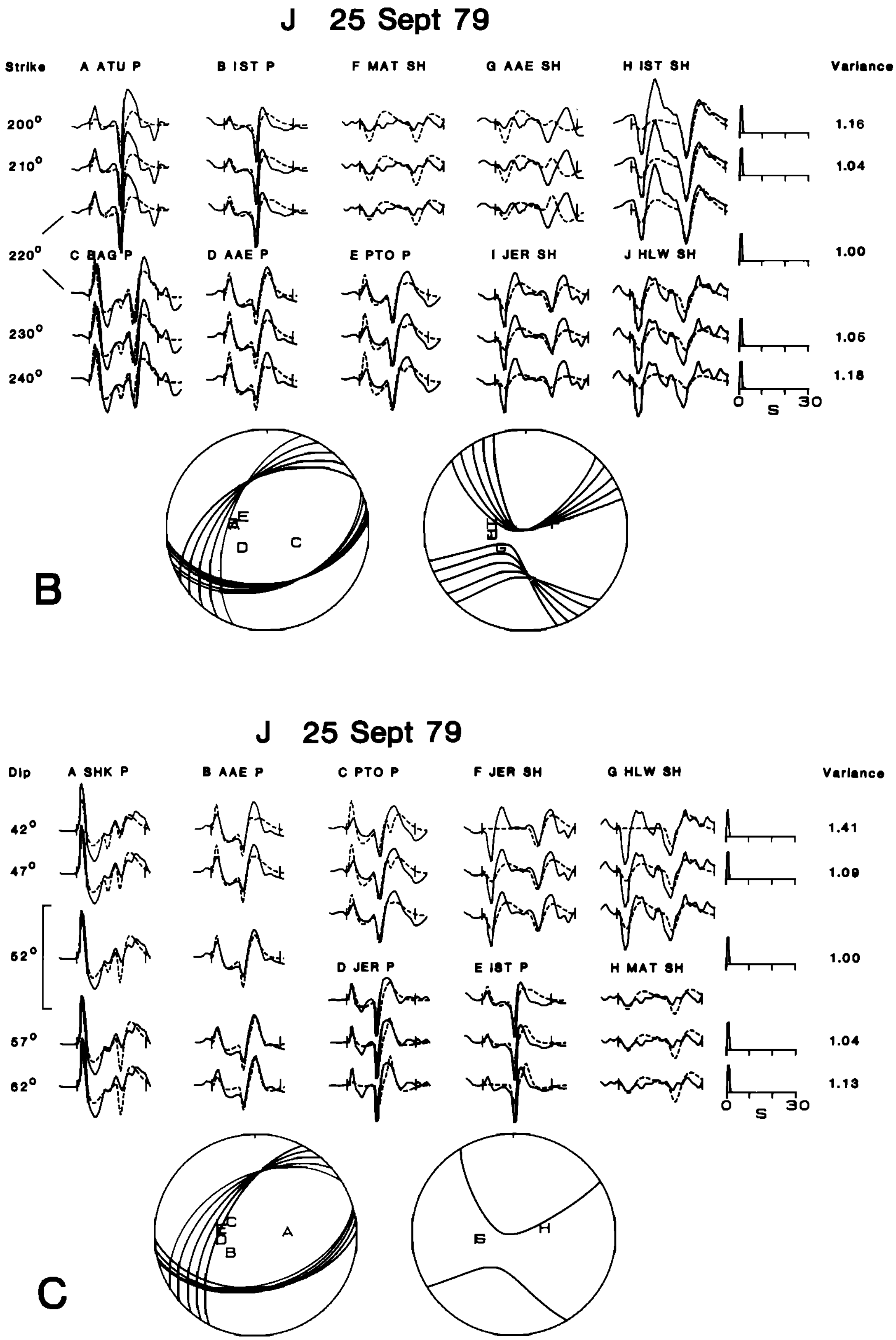

Fig. 19. (continued)

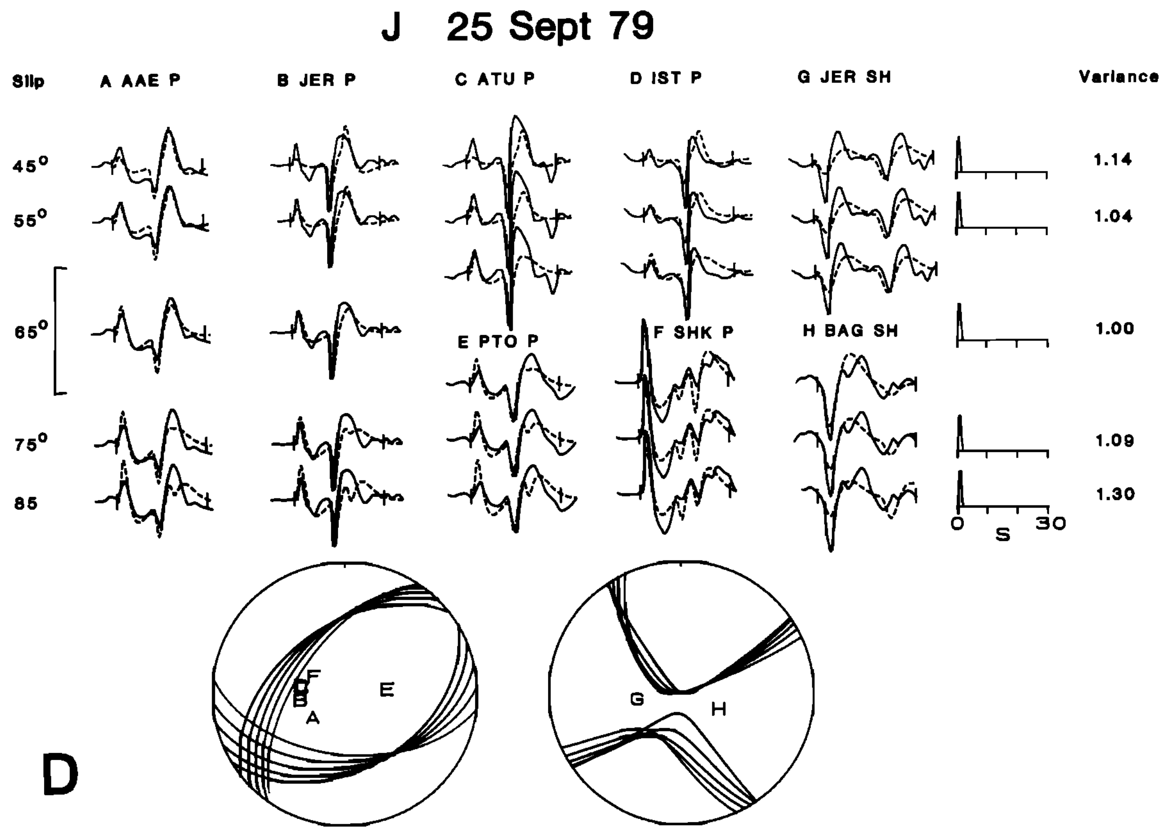

Fig. 19. (continued)

physically reasonable limits. The instrument response for WWSSN seismographs is known well, and the instruments are calibrated often. We use the causal attenuation operator of Futterman [1962] with a t^* of 1 s for P waves and 4 s for SH waves ($t^* = t/Q$, where t is the travel time and Q is the averaged attenuation along the ray path). These values are within 10% of those estimated for the mantle [e.g., Dziewonski and Anderson, 1981]. Experiments in which t^* was varied by a factor of 2 showed that the fault plane solution and the centroid depth were not sensitive to the attenuation operator because the inversion routine simply compensates by changing the source duration and the seismic moment. The assumed receiver structure, a half-space with v_p = 6.0 km/s, v_s = 3.4 km/s, density = 2700 kg/m^3, is an approximation to the average velocity structure beneath the various stations. Because the inversion routine is sensitive only to coherent signals in the waveforms, we expect that receiver structure will not bias the solution as it is unlikely that all receivers have a similar velocity structure.

The seismic source is approximated by a point double-couple, which appears to be valid for the relatively short durations of the earthquakes studied. Nabelek [1984] showed that when using WWSSN long-period data, a point source is a good approximation for earthquakes with fault dimensions of 25 by 11 km^2 and a source duration of 9 s. The earthquakes studied here have much shorter source durations (all but two are less than 5 s) and probably have fault rupture areas of less than 100 km^2.

Two additional parameters that must be determined are the P and SH arrival times. These were initially picked using the ISC location and the Jeffreys-Bullen (J-B) travel time tables. The arrival times were later adjusted by cross-correlating the observed seismogram with the synthetic waveform. The adjusted arrival time and the time predicted by the J-B tables rarely disagreed by more than 3 s for P waves and more than 9 s for SH waves.

Due to background noise on the seismogram, the distribution of stations, and unmodeled contributions to the observed seismograms, there typically is an adequate fit between the synthetic and recorded seismograms for a range of source parameters. To examine the resulting uncertainties, each source parameter was fixed at values bracketing its best fit value, the inversion routine was rerun while allowing the other parameters to change, and the new best fit synthetic waveforms were compared to the observed seismograms (see Figures 19 and 20). In this way we estimated the uncertainties to be ±5° in dip, ±10° in strike, ±15° in rake, and 3 km in centroid depth. These uncertainties include the effects of trade-offs among the parameters since all the parameters but one were left free to change during these tests.

Earthquake J of September 25, 1979, is representative of the deeper thrust events studied (e.g., A, G, J, and K). It has simple waveforms indicative of a simple source time function (Figure 19a). For each row in Figure 19a the depth was held fixed and the fault plane solution and source time function were allowed to

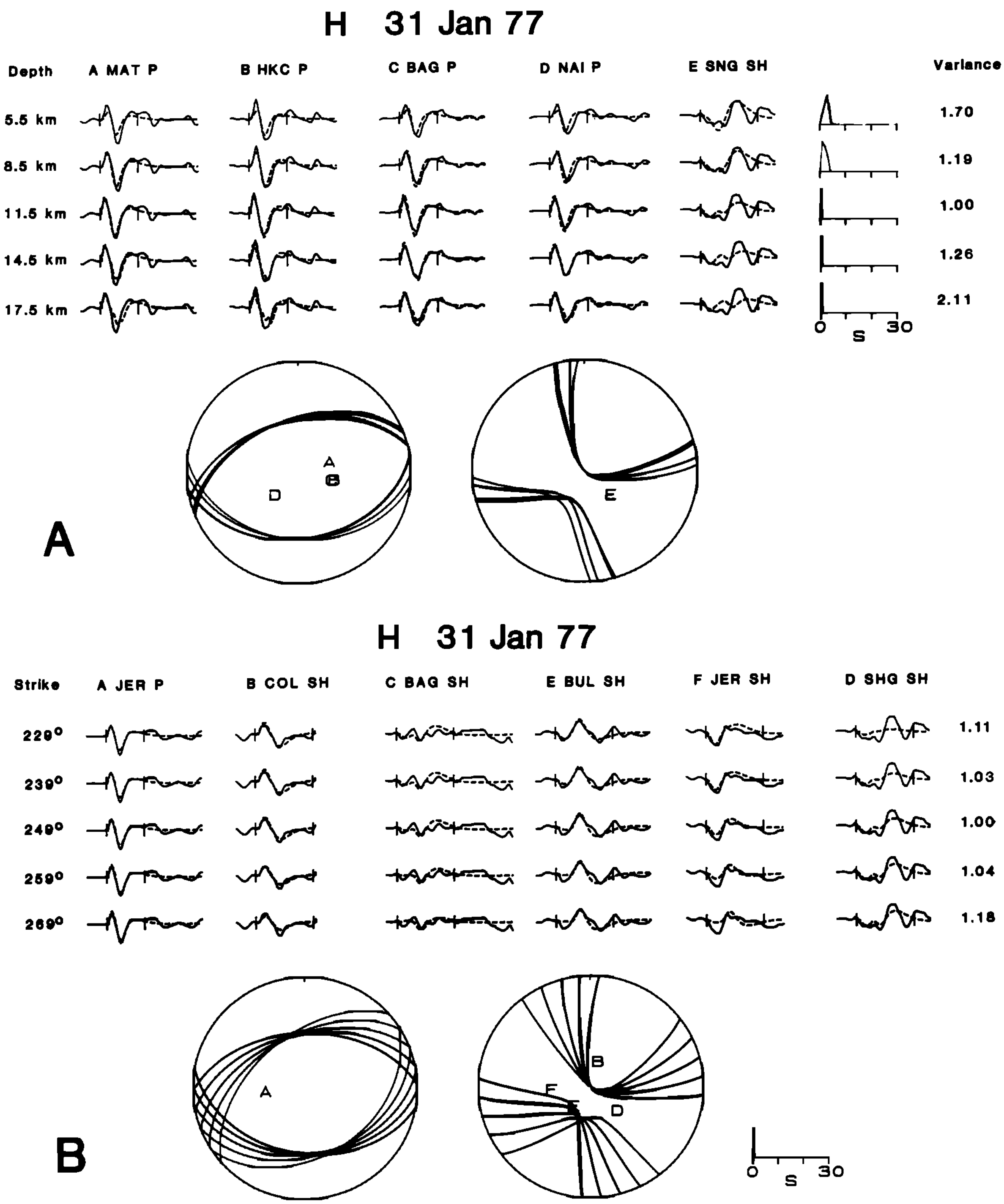

Fig. 20. Diagrams illustrating the uncertainty in inversion parameters for the best-fitting focal mechanism for earthquake H of January 31, 1977. Format as in Figure 19. (a) depth, (b) strike, (c) dip, (d) slip.

vary. The timing of the reflected phases is not matched for values of focal depth 6 km above and below the best fit depth. Even for depths of 37 and 43 km, there is a consistent mismatch between the synthetic and the observed seismograms (Figure 19a), which is confirmed by the increase in variance. Note that the fault plane solution is stable despite the variation in depth and source time function.

The centroid depth is constrained largely by the P waveforms (Figure 19a), while the SH waveforms are more sensitive to the strike, dip, and rake angles (Figures 19b-19d). In general, the stations nearest the P and SH nodal surfaces are most sensitive to changes in the orientation of the nodal planes. For instance, in Figure 19b, synthetic SH waveforms for station IST change markedly as the strike changes from 200°

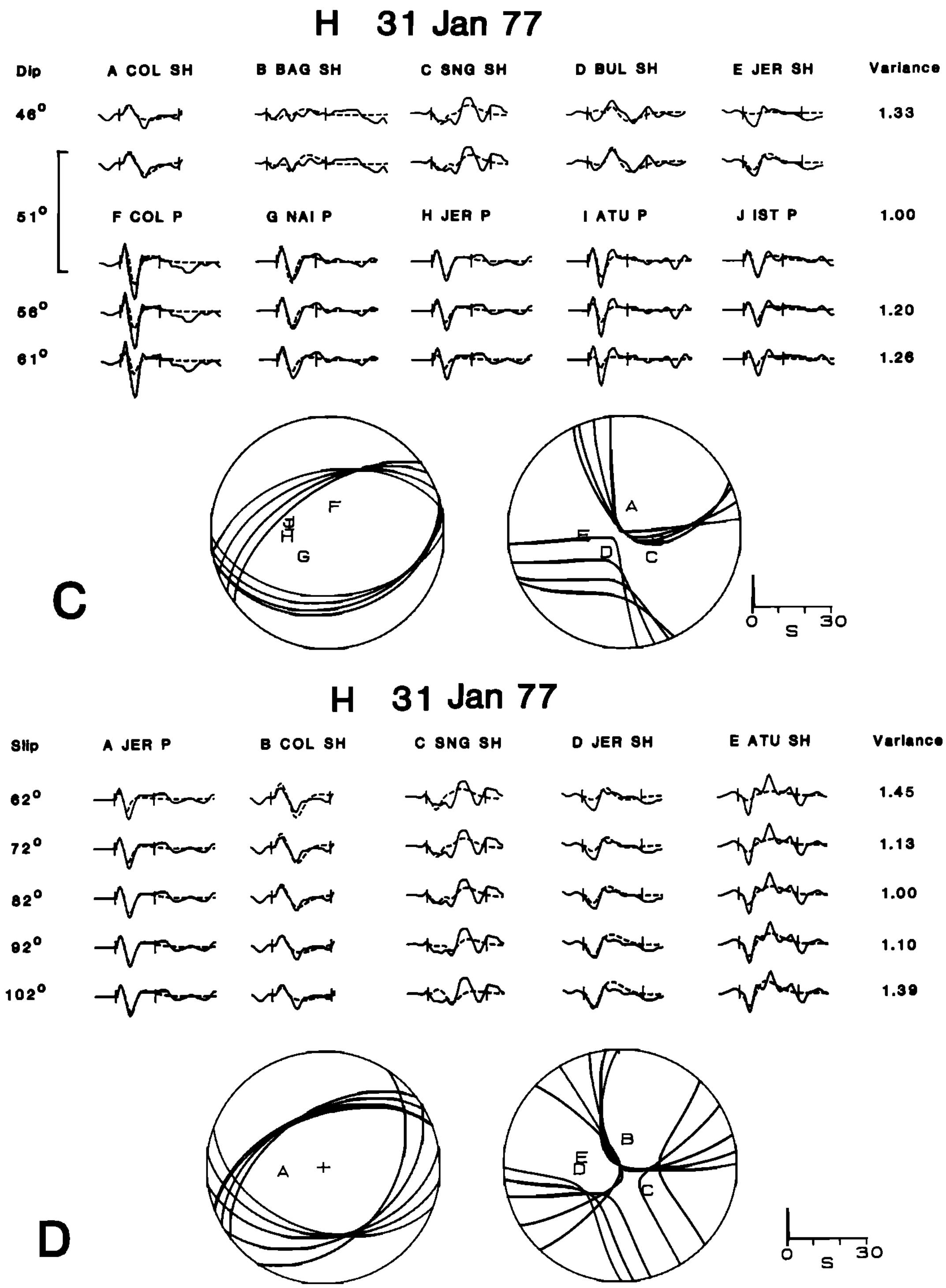

Fig. 20. (continued)

to 220°, but for strikes of 220°-240° the rays to this station are far from the SH nodal surface and the waveforms change very little and so are not shown. The JER and HLW seismograms, however, constrain the strike to be less than about 230°. Thus the strike is constrained to be between 210° and 230°. The pairs of stations ATU and IST and JER and HLW plot at almost identical points on the focal sphere so that the difference in waveforms at these pairs of stations reveal to some degree the character of the "noise" present in the data. The waveforms shown in Figure 19c show how the dip angle is constrained to be 47°-57°, primarily by the amplitude of the first-arriving P and SH waves at stations near the nodal surfaces. The slip is likewise constrained to be between 50° and 80° (Figure 19d).

A similar set of plots is shown for earthquake H of January 31, 1977, a relatively shallow event with a simple time function, typical of many of the earthquakes studied (Figure 20). Here, too, the timing of the reflected P phases constrains the centroid depth. Even for a 1-s source duration, at a depth of 17.5 km the synthetic waveforms are too broad due to the late arriving reflected phases. The P/SH amplitude ratio also constrains the depth. For shallow events with this type of mechanism the P and pP phases interfere destructively, while the S and sS waves interfere constructively, so that the P/SH amplitude ratio decreases with decreasing focal depth. The best fitting solution with the depth fixed at 5.5 km produces P wave amplitudes that are too small relative to the SH wave amplitudes. This shows the importance of using the amplitudes, and not just the shape, of the waveforms in the inversion. The remaining plots show that the SH waveforms are particularly useful in constraining the orientation of the fault plane solution. For thrust earthquakes like this one, the P waveforms are rather insensitive to changes in the orientation of the nodal planes (compare synthetic waveforms for JER in Figure 20b). In contrast, many of the stations fall near the SH nodal surfaces.

For each earthquake many more solutions were generated than are presented here. These experiments lead us to quote uncertainties of ±5° in dip, ±10° in strike, ±15° in rake and 3 km in centroid depth for these thrust earthquakes. In addition, as explained above, uncertainties in the velocity structure contribute an additional ±10% uncertainty in the centroid depth.

Acknowledgments. We wish to thank John Nabelek and Geoff Abers for helping with the development of the computer software used in this study. Geoff Abers and Craig Jones made helpful suggestions, and Brian Evans provided useful computer hardware and software. James Ni, Terry Wallace, and Douglas Wiens suggested several useful improvements to the original manuscript. This work was supported in part by National Science Foundation grant 8500810-EAR and NASA grant NAG4-795.

References

Aki, K., and P. G. Richards, Quantitative Seismology - Theory and Methods, 932 pp., W. H. Freeman, San Francisco, Calif., 1980.

Bird, P., Laramide crustal thickening event in the Rocky Mountain foreland and Great Plains, Tectonics, 3, 741-758, 1984.

Burchfiel, B. C., and G. A. Davis, Nature and controls of Cordilleran orogenesis, western United States: Extension of an earlier synthesis, Am. J. Sci., 272, 97-118, 1975.

Burtman, V. S., Structural geology of the Variscan Tien Shan, Am. J. Sci., 275A, 157-186, 1975.

Burtman, V. S., Faults of Middle Asia, Am. J. Sci., 280, 725-744, 1980.

Chen, W.-P., and P. Molnar, Seismic moments of major earthquakes and the average rate of slip in central Asia, J. Geophys. Res., 82, 2945-2969, 1977.

Dickinson, W. R., and W. J. Snyder, Plate tectonics of the Laramide orogeny, Mem. Geol. Soc. Am., 151, 355-366, 1978.

Dmitriyev, M. I., M. A. Demtchenko, and I.I Lando, The Central Tien Shan, Report of the Ukrainian Scientific Expedition to the Central Tien Shan (in Ukrainian), 551 pp., Radianska Shkola, Kharkov, 1935.

Dziewonski, A. M., and D. L. Anderson, Preliminary reference Earth model, Phys. Earth Planet. Inter., 25, 297-356, 1981.

Engebretson, D. C., A. Cox, and G. A. Thompson, Correlation of plate motions with continental tectonics: Laramide to Basin-Range, Tectonics, 3, 115-119, 1984.

England, P., and G. Houseman, The role of lithospheric strength heterogeneities in the tectonics of Tibet and neighboring regions, Nature, 315, 297-301, 1985.

England, P., and G. Houseman, Finite strain calculations of continental deformation, 2, Comparison with the India-Asia collision zone, J. Geophys. Res., 91, 3664-3676, 1986.

Futterman, W. I., Dispersive body waves, J. Geophys. Res., 67, 5279-5291, 1962.

Gamburtsev, G. A., P. S. Veitsman, and Yu. V. Tulina, Structure of the crust in the northern Tien Shan according to data from deep seismic sounding, Dokl. Akad. Nauk SSSR, 105, 83-86, 1955.

Gröber, P., Der Südliche Tiën-Schan, 110 pp., B. G. Teubner, Leipzig, 1914.

Krestnikov, V. N., History of oscillatory movements in the Pamirs and adjacent regions of Asia, 199 pp., Akademii Nauk SSSR Press, Moscow, 1962.

Langston, C. A., and D. V. Helmberger, A procedure for modelling shallow dislocation sources, Geophys. J. R. Astron. Soc., 42, 117-130, 1975.

Leith, W., and A. Teremetsky, Trenching and geomorphological studies of the Talas-Fergana fault, Soviet Central Asia, Eos Trans. AGU, 67, 375, 1986.

Molnar, P., and P. Tapponnier, A possible dependence of tectonic strength on the age of the crust in Asia, Earth Planet. Sci. Lett., 52, 107-114, 1981.

Molnar, P., T. J. Fitch, and F. T. Wu, Fault plane solutions of shallow earthquakes and contemporary tectonics in Asia, Earth Planet. Sci. Lett., 19, 101-112, 1973.

Nabelek, J., Determination of earthquake source parameters from inversion of body waves, Ph.D. thesis, 361 pp., Mass. Inst. of Technol., Cambridge, 1984.

Nabelek, J., Geometry and mechanism of faulting of the 1980 El Asnam, Algeria, earthquake from inversion of teleseismic body waves and comparison with field observations, J. Geophys. Res., 91, 12,713-12,728, 1985.

Ni, J., Contemporary tectonics in the Tien Shan Region, Earth Planet. Sci. Lett., 41, 347-354, 1978.

Norin, E., Geology of Western Quruq Tagh, E. Tien Shan, 194 pp., Tryckeri Aktiebolaget Thule, Stockholm, 1937.

Norin, E., Geologic Reconnaissances in the Chinese Tien Shan, 229 pp., Tryckeri Aktiebolaget Thule, Stockholm, 1941.

Smithson, S. B., J. A. Brewer, S. Kaufman, J. Oliver, and C. Hurich, Structure of the Laramide Wind River uplift, Wyoming, from COCORP deep reflection data and gravity data, Geology, 6, 648-652, 1980.

State Seismological Bureau of China, Isoseismal maps of earthquakes in China, 107 pp., Seismology Publishing House, Beijing, 1979.

Suvorov, V. P., Main faults of Kazakhstan and

Central Asia, Faults and Horizontal Movements of the Earth's Crust, Tr. Geol. Inst. Akad. Nauk SSSR, 80, 173-237, 1963.
Tapponnier, P., and P. Molnar, Slip-line field theory and large scale continental tectonics, Nature, 264, 319-324, 1976.
Tapponnier, P., and P. Molnar, Active faulting and Cenozoic tectonics of the Tien Shan, Mongolia, and Baykal regions, J. Geophys. Res., 84, 3425-3459, 1979.
Terman, M. J., C. C. Woo, D. C. Alverson, D. P. Cox, and A. J. Woloshin, Atlas of Asia and Eastern Europe - To support detection of underground nuclear testing, vol. 2, Tectonics, U.S. Geological Survey, Reston, Va., 1967.
Trifonov, V. G., Late Quaternary tectonic movements of western and central Asia, Geol. Soc. Am. Bull., 89, 1059-1072, 1978.
Vilkas, A., Sismicité et tectonique du Tien Shan: Etude de quelques séismes par la méthode des sismogrammes synthétiques, M. S. thesis, 172 pp., Univ. of Paris, Paris, 1982.
Vinnik, L. P., and A. M. Saipbekova, Structure of the lithosphere and the asthenosphere of the Tien Shan, Ann. Geophys., 2, 621-626, 1984.
Vol'vovskii, I. S., and B. S. Vol'vovskii, Cross-Sections of the Earth's Crust in the Territory of the USSR, Plotted From Deep Seismic Soundings, 268 pp., Sovetskoe Radio, Moscow, 1975.
Wallace, R. E., The Talas-Fergana fault, Kirghiz and Kazakh, USSR, Earthquake Info. Bull., 8, 4-13, 1976.
Wesson, R. L., I. L. Nersesov, and F. G. Fischer, Seismicity and focal mechanism study in Peter the First Range, Tadzhik SSR, Eos Trans. AGU, 56, 1025, 1975.
Zhang, Zh. M., J. G. Liou, and R. G. Coleman, An outline of the plate tectonics of China, Geol. Soc. Am. Bull., 95, 295-312, 1984.

R. McCaffrey, P. Molnar, and M. R. Nelson, Department of Earth, Atmospheric, and Planetary Sciences, MIT 54-712, Cambridge, MA 02139.

(Received January 5, 1987;
revised June 25, 1987;
accepted July 6, 1987.)